NANO LETTERS

pubs.acs.org/NanoLett

Defects in Individual Semiconducting Single Wall Carbon Nanotubes: Raman Spectroscopic and in Situ Raman Spectroelectrochemical Study

Martin Kalbac,*,†,‖ Ya-Ping Hsieh,† Hootan Farhat,‡ Ladislav Kavan,‖ Mario Hofmann,† Jing Kong,† and Mildred S. Dresselhaus†,§

†Department of Electrical Engineering and Computer Science, ‡Department of Materials Science and Engineering, and §Department of Physics, Massachusetts Institute of Technology, Cambridge, Massachusetts 02139, United States and ‖J. Heyrovský Institute of Physical Chemistry, v.v.i., Dolejškova 3, CZ-18223 Prague 8, Czech Republic

ABSTRACT Raman spectroscopy and in situ Raman spectroelectrochemistry have been used to study the influence of defects on the Raman spectra of semiconducting individual single-walled carbon nanotubes (SWCNTs). The defects were created intentionally on part of an originally defect-free individual semiconducting nanotube, which allowed us to analyze how defects influence this particular nanotube. The formation of defects was followed by Raman spectroscopy that showed D band intensity coming from the defective part and no D band intensity coming from the original part of the same nanotube. It is shown that the presence of defects also reduces the intensity of the symmetry-allowed Raman features. Furthermore, the changes to the Raman resonance window upon the introduction of defects are analyzed. It is demonstrated that defects lead to both a broadening of the Raman resonance profile and a decrease in the maximum intensity of the resonance profile. The in situ Raman spectroelectrochemical data show a doping dependence of the Raman features taken from the defective part of the tested SWCNT.

KEYWORDS Single wall carbon nanotubes, Raman spectroscopy, defects, spectroelectrochemistry

Defects in a single-walled carbon nanotube (SWCNT) can exhibit new interesting properties. For example, defects are reactive centers on a nanotube so that they can be used as the sites for nanotube decoration or to improve the sensing of the attached species.[1] Therefore a better understanding of the role of defects in SWCNTs can open a route toward engineering the properties of new electronic devices based on carbon nanotubes by controlling or creating defects.

Defects can be studied by a number of experimental methods: X-ray photoelectron spectroscopy,[2] transmission electron microscopy,[3] Raman spectroscopy,[4−10] optical spectroscopy,[11] or scanning tunneling microscopy (STM).[12] Raman spectroscopy has found wide use in the evaluation of the defects of graphite-like carbons in general and of SWCNTs in particular. The so-called D band in the Raman spectra of sp^2 carbons is a signature of defects in the graphene lattice.[13] Hence, perfect graphite/graphene, is assumed to show no D band. The D mode originates from a double-resonance Raman scattering process.[14,15] In this process, the incident photon resonantly excites an electron−hole pair. The electron is subsequently scattered under emission/absorption of a phonon. To satisfy momentum conservation, the electron has to be scattered back to a point in k-space where its momentum is near that of the initial hole. For the D mode in the Raman spectrum, the backscattering is achieved by a defect.

Other important Raman features of carbon nanotubes include the radial breathing mode (RBM), the tangential mode (G) and the G′ mode. The G′ mode normally does not involve any elastic process, but for some disordered systems the scattering process can been seen in the second order spectra and in such a cases this feature can be called a 2D feature. The RBM band is of particular importance since its frequency scales with tube diameter d_t according to the relation

$$\omega_{RBM} = \frac{C_1}{d_t} + C_2 \qquad (1)$$

where the constant C_1 has been reported to be in the range of 217 to 227 $cm^{-1}\cdot nm$ (refs 16 and 17). The constant C_2 ($\sim$15 cm^{-1}) is generally used to include the effect of environmental interactions, that is, between nanotubes in bundled samples and between nanotubes and substrates, and therefore in the case of individual isolated tubes, it is expected to be zero when they are suspended. For small diameter tubes, a knowledge of the diameter (as obtained from the ω_{RBM}) and

* To whom correspondence should be addressed. E-mail: kalbac@mit.edu.
Received for review: 08/3/2010
Published on Web: 10/12/2010

DOI: 10.1021/nl102727f | *Nano Lett.* **2010,** *10,* 4619–4626

the resonance profile is sufficient to locate it on the Kataura plot and to determine the chiral indicies (n,m) of a particular nanotube.

The tangential mode (G band) consists of six Raman-active lines for chiral nanotubes with symmetries: $2A_{1g} + 2E_{1g} + 2E_{2g}$. These six lines are reduced to three Raman-active bands for zigzag and armchair tubes. Furthermore, the E_1 and E_2 symmetry modes have a much weaker Raman intensity than the totally symmetric A_1 modes.[18] Thus only two components of the G mode are usually considered in the analysis. The G band intensity is assumed not to be dependent on defects, and thus the I_D/I_G intensity ratio has been used for the evaluation of the defect density since the time of earliest reported Raman studies of graphite.[13] The I_D/I_G ratio is also frequently correlated with the size L_a of a graphite crystal.[13] The G′ band is used as another reference mode which results from a two phonon, second-order symmetry-allowed Raman process and it presumably occurs independently of structural defects.[14,19] We show in our study nevertheless that the intensity and line width of the G′ band is affected by defects.

Despite the large number of experimental results on the defect-induced changes to the Raman spectra of bundled nanotubes samples the information that can be extracted from such analyses is limited and thus many issues remain unclear. In particular, it is difficult to explore the influence of defects on other Raman features (beyond the D mode) in ensemble measurements, since the D band cannot be correlated with any individual nanotube and other Raman features of that nanotube. In other words, a large observed D-band intensity in a Raman spectrum might originate from one nanotube, while the RBM or G-band could stem from another tube present in the same ensemble of nanotubes. Additionally, the presence of carbon impurities (amorphous carbon, multiwalled carbon nanotubes) in a sample can lead to a strong D band, which can make the interpretation of experimental results more difficult. For example, it has been shown that chemical treatment can lead to the selective destruction of nanotubes with a specific diameter.[20] The product of this decomposition of SWCNTs is usually amorphous carbon that will contribute to the D band significantly. Until now it has not been possible to distinguish between the contribution to the D band from amorphous carbon and that coming from defects associated with defective nanotubes. In contrast, for individual tubes the D-band, if at all present, can be studied directly. Therefore, studies on individual tubes are highly desirable.[7]

Here we have studied long (more than 1 mm) individual semiconducting single-walled carbon nanotubes that were intentionally and only locally modified by defects while other parts of the tube remained defect-free. The approach adopted in the present work allows the influence of the defect to be studied in the most straightforward and definitive way. Hence, we have been able to follow changes in the intensity of all Raman bands, their frequency shifts and also changes in the resonance Raman profile due to the creation of defects in localized regions of individual tubes.

SWCNTs were synthesized directly on a SiO_2/Si substrate using Fe as a catalyst. The defects on the SWCNT were created by using an RF Ar plasma in a UHV chamber. The sample was irradiated for 5s using a plasma at 57 V, 4 W power level and an Ar pressure of 30 mTorr. For the electrochemical charging experiments, SWCNTs were subsequently contacted using Au evaporated on a part of the substrate, and the evaporated Au served as a working electrode. The cell was completed with a Pt-counter electrode and an Ag-wire pseudoreference electrode. The electrolyte gel was 0.1 M $LiClO_4$ dissolved in dry propylenecarbonate/poly(methyl methacrylate) (PMMA, Aldrich). Electrochemical charging of the working electrode on which SWCNTs were placed was carried out by varying the applied potential V_e between -1.5 and 1.5 V versus an Ag pseudoreference electrode (PAR potentiostat). Note that we used a three electrode system and we make our measurements in the potentiostatic regime, so that no current is flowing between the pseudoreference and the working electrode during the measurement. Consequently the environment of the pseudoreference electrode is not changed during the measurement and a stable potential for our pseudoreference electrode is ensured. The Raman spectra were excited by a dye laser (R6G dye, Coherent), a Ti-Sapphire laser (Coherent), or a Nd:YAG laser (Coherent). The spectrometer resolution was about 5 cm^{-1}. The spectrometer was interfaced with a microscope (Carl-Zeiss, objective 100×). The diameter of the laser spot was about 500 nm.

Figure 1 shows the SEM and AFM images of individual SWCNTs grown directly on a Si/SiO_2 substrate by chemical vapor deposition (CVD). The nanotubes in this image are typically parallel to each other and aligned with the gas flow.[21] The distance between adjacent SWCNTs is usually greater than 10 μm. This geometry simplifies finding a tube by the Raman microscope and also enables alignment of the laser polarization parallel to the SWCNT axis, which is important for obtaining a reasonably strong Raman signal and for establishing a well-defined reproducible geometry for efficient and reproducible data collection. For our analysis, we explicitly selected spectra for which only one RBM band occurred in the spectrum. Also several laser lines were used as probes to ensure that the laser spot does not contain several tubes.

As mentioned above we used radiofrequency (RF) Ar plasma etching of the as-grown nanotubes to create localized defects. Because of the nanotube's macroscopic size (exceeds 1 mm, see Figure 1), it is possible to protect a part of the SWCNT by a shadow mask. An example of the Raman spectrum of a partially defective individual nanotube, is shown in Figure 2. The spectra are excited using 2.05 eV (Figure 2A) and 2.10 eV (Figure 2B) laser excitation energies. The defective part of the nanotube is clearly identified by

DOI: 10.1021/nl102727f | Nano Lett. 2010, 10, 4619–4626

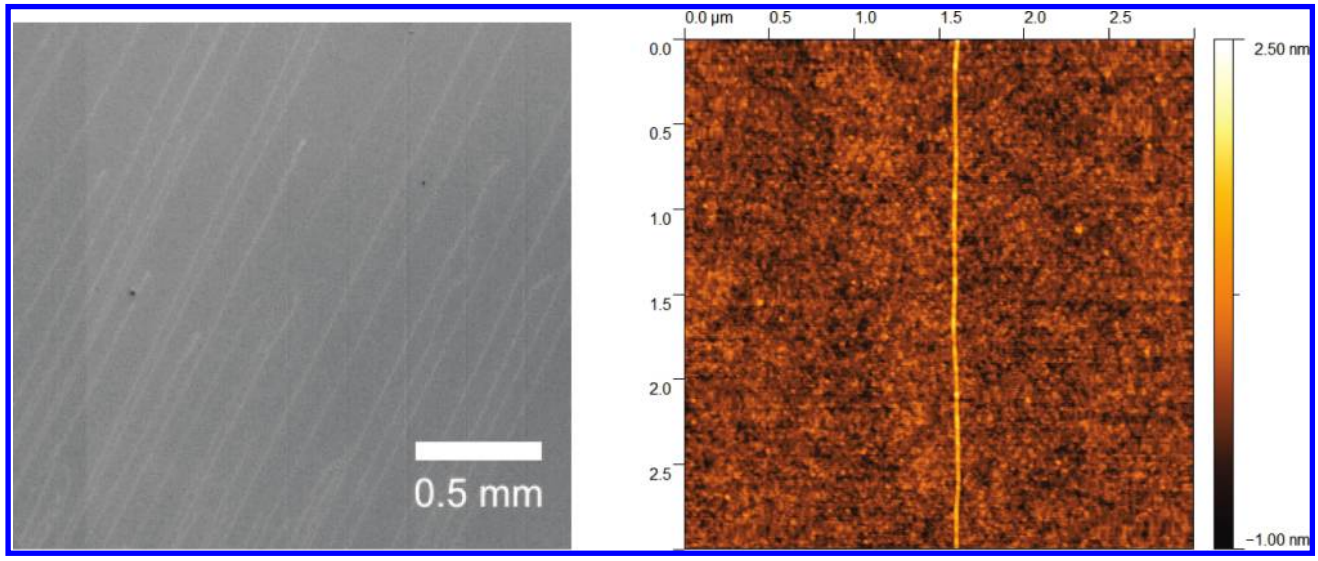

FIGURE 1. An SEM image of individual tubes grown on a SiO_2/Si substrate (left), an AFM image of an individual tube (right). The color scale bar in the right panel indicates the height of the features.

the D band at about 1340 cm^{-1}. In contrast, the pristine part of the same individual nanotube does not exhibit any significant D band. The nanotube ends are located away from the laser spot so they do not contribute to either of the Raman spectra in Figure 2. This is in contrast to previous measurements on nanotube bundles where both the tube side wall and tube ends of the same and different tubes were in the laser spot and their individual contribution to the D band could not be distinguished in the Raman spectra. In addition, for the experiment on individual SWCNTs it is clear that the D mode is coming solely from the carbon nanotube and is not coming from carbon impurities since the RBM mode is still present indicating the persistence of the nanotubes. The I_D/I_G ratio is about 0.1, which indicates a relatively low defect density. According to the recent studies on graphene,[22] the average distance between defects may be estimated as 25 nm for the samples studied in this work using the $I_D/I_{G'}$ ratio.

As shown in Figure 2, the appearance of the D band is not the only signature of defect formation in the Raman spectra. There is also a change of the intensity of all the Raman features and line shapes for the G and the G′ Raman bands. The RBM, the G band and the G′ Raman band all decrease in intensity for the defective part of the nanotube when compared to the pristine part. The changes of the intensity and line shape generally differ for different bands and the changes to each of the features are also dependent on the laser excitation energy. For the particular nanotube shown in Figure 2, the Raman intensities of the RBM, G^+ and G′ modes for the defective part are reduced approximately by a factor of 2 for the 2.05 eV laser excitation energy (Figure 2A). The G^- band almost vanishes for the part of SWCNT showing a strong D-band feature. For the laser excitation energy 2.05 eV, the tube is close to the resonance maximum (E_{33}^S). If the Raman spectra are measured slightly off-resonance, the reduction of the intensities of the G-band features is much less pronounced but starting from a lower base intensity. This is demonstrated in Figure 2B where the Raman spectra of the pristine and defective parts of the tube excited at the 2.10 eV laser excitation energy are shown (the nanotube is the same as in Figure 2A). The exception from this trend is the G^- band, which again almost vanishes, for the part of the SWCNT showing a strong D-band feature.

In contrast to the significant change of the intensity, the peak frequency, and the line width of the RBM are not influenced by the presence of defects. This is in agreement with theoretical calculations[23] and can be explained by the fact that the RBM is a uniform radial displacement of the atoms, and therefore it depends only slightly on the atomic structure and is insensitive to small deviations of the nanotube surface from the ideal cylinder.[23] However, the defective part of the nanotubes exhibits a change of the G-mode line shape compared to the pristine part of the tube, since the lower frequency G^- part of the G mode is more significantly reduced in intensity than the higher frequency G^+ part. Nevertheless, the frequency of the G^+ part is not changed upon defect formation. This is in contrast to the theoretical prediction.[23] However, the calculations were performed for a relatively small diameter tube where the effects of defects can be much more pronounced due to the larger curvature of small diameter tubes.[23]

The behavior of the G′ mode is of particular importance since the $I_D/I_{G'}$ intensity ratio is also used for the evaluation of the number of defects in SWCNTs.[19] As can be seen in Figure 2 the creation of defects leads to a decrease in the G′ mode intensity and also a broadening and a small downshift in the frequency of the G′ band. The decrease of the intensity of the G′ mode upon defect creation increases the $I_D/I_{G'}$ intensity ratio, which could lead to an overestimation of the amount of defects if this effect is not accounted for. This

DOI: 10.1021/nl102727f | *Nano Lett.* **2010,** *10,* 4619–4626

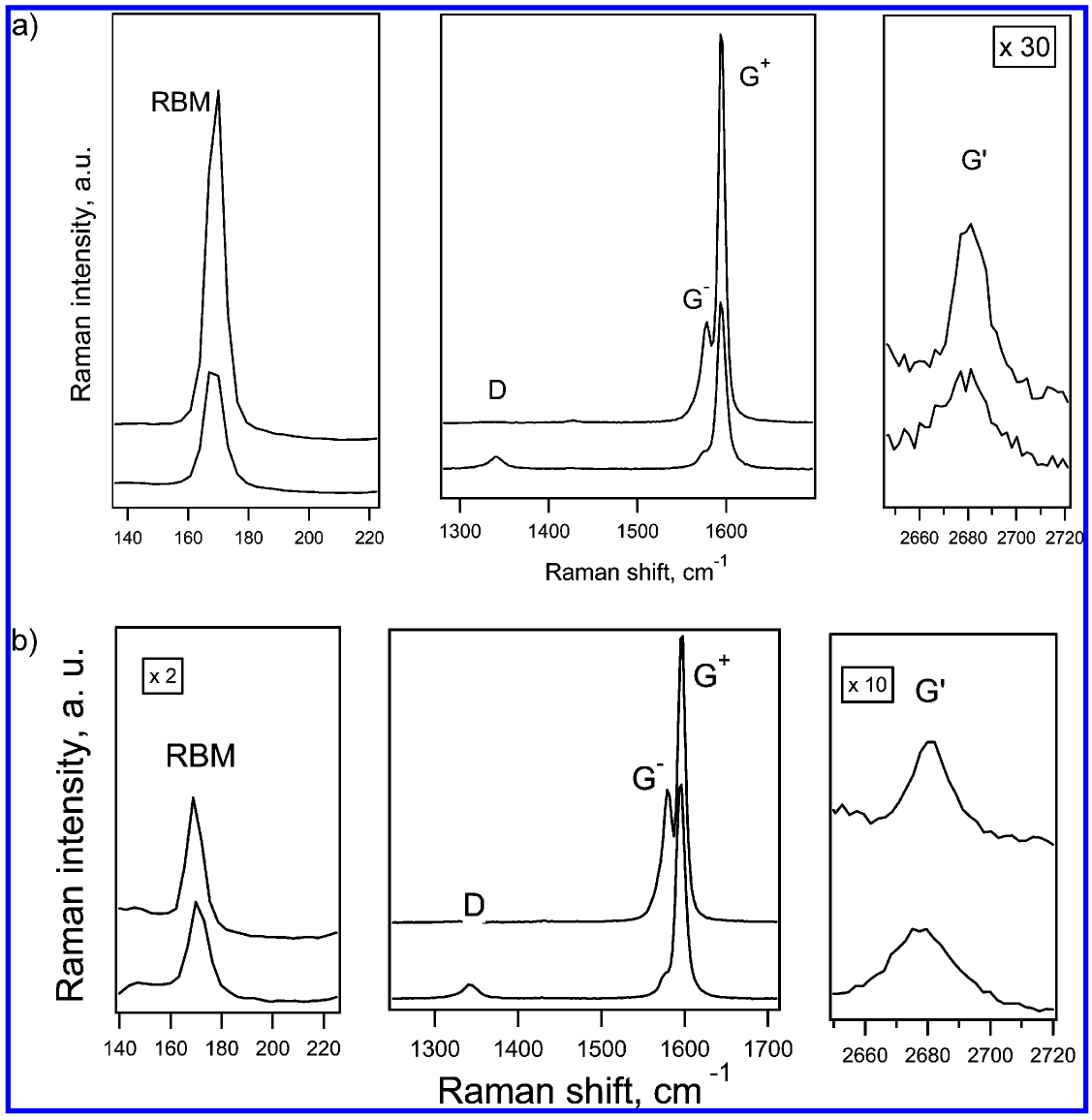

FIGURE 2. (A) Raman spectra of the pristine part (top) and the defective part (bottom) of the same individual SWCNT. The spectra are excited by 2.05 eV laser excitation energy. (B) Raman spectra of the pristine part (top) and the defective part (bottom) of the same individual SWCNT as in (A). The spectra are excited by 2.10 eV laser excitation energy.

overestimation can be alleviated if the area of the G′ band is used. Nevertheless even the area under the G′ band feature is smaller for the defective part of the nanotube by a factor of about 2. The changes in the G′ mode have been studied recently on substitutionally doped SWCNTs.[4] It was shown that defective tubes exhibit a new downshifted component of the G′ mode which is a consequence of the phonon renormalization at defective sites.[4] In this study, we could not distinguish between the two components contributing to the G′ mode due to the low intensity/small downshift of the defect-induced band but the broadening of the G′ mode for the case of a defective tube could indicate the appearance of a lower frequency defect induced component.

It has been also suggested by theoretical calculations[23] that the creation of defects can result in the appearance of new features in the Raman spectra. These new features include a low frequency deformation mode and also a high frequency defect-associated mode. However, we did not observe either of these new types of Raman bands after the creation of defects. Furthermore, there is no signature of any D′ band intensity (around 1620 cm^{-1}), which is often observed in defective graphene samples.[22] The discrepancy between experimental results and theoretical expectations could be explained in several ways. The high-frequency defect-associated mode could overlap with the G^+ mode and therefore could not be resolved or identified. On the other hand, the low frequency mode could be too close to the Raman excitation laser wavelength and thus it could be cut out from our experiment by the Raman filter in our experimental setup. Another reason could be the relatively large diameter of the studied nanotube. The calculation[23] was performed for a (7,0) tube with a diameter of about 0.55 nm,

DOI: 10.1021/nl102727f | Nano Lett. 2010, 10, 4619–4626

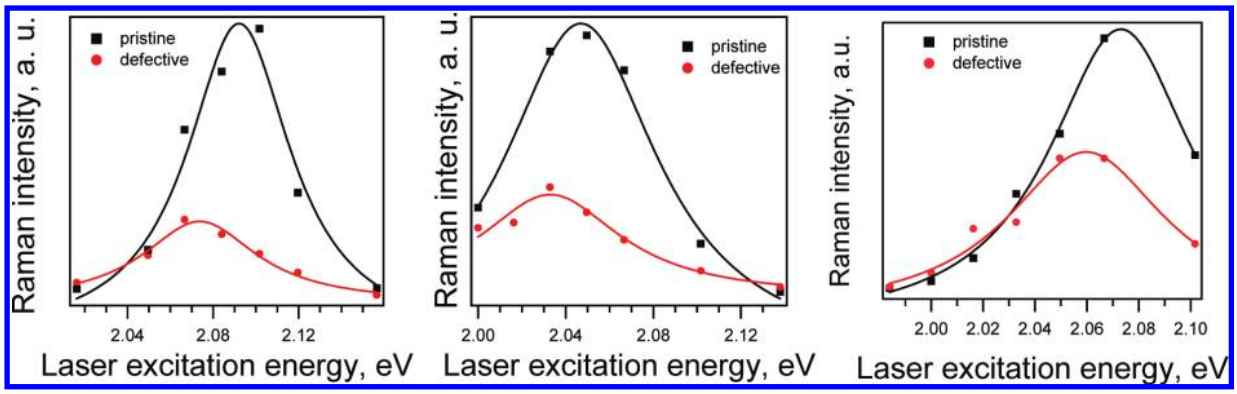

FIGURE 3. Plots of the dependence of the Raman intensity of the RBM mode on laser excitation energy for three different individual semiconducting nanotubes. The RBM frequencies were 150, 170, and 130 cm^{-1} for the left, middle, and right plots, respectively. Squares represent the pristine part of each individual nanotube, while circles correspond to the defective part of the same individual nanotube. The solid lines represent the Lorentzian fits to the experimental points.

while the smallest nanotube in our study has a diameter of about 1.3 nm as approximated from the measured RBM band frequencies (~170 cm^{-1}) using eq 1 with $C_1 = 227$. (The smaller diameter individual nanotubes were not available under the growth conditions used.)

To gain a deeper understanding of the attenuation of the Raman spectra caused by the formation of defects, we measured the resonance Raman profile for the pristine and defective parts of the nanotube. The results for three different tubes are shown in Figure 3. The RBM frequencies of the tubes shown on Figure 3 were 150, 170, and 130 cm^{-1} for left, middle, and right plot, respectively. The resonance profiles have been analyzed for the RBM band since it is more sensitive to the change of the laser excitation energy than for other Raman features.[24] It can be clearly seen that the intensity of the Raman spectra at the maximum of the resonance profile of the pristine part is stronger than in the case of the defective part for all three tested tubes. The decrease of the intensity at the resonance maxima varies slightly between different tubes, but in general the intensity of the defective parts of the tubes is decreased by a factor of 2−3 compared to the pristine parts. This trend is in rough qualitative agreement with theoretical calculations[23] although the spectral intensity was predicted to be reduced by a factor of 4−15, depending on the type of the defect. We did not observe a dramatic influence of the diameter of these nanotubes on the change of the resonance Raman profile after defect creation. Only the resonance profile of the widest diameter tube seems to be less affected by the defect. This could be understood by taking into account the lower structural tension in the large diameter tubes. Nevertheless, more experiments must be done to fully understand the role of the nanotube diameter in the defect creation and/or the appearance of defect signatures in the Raman spectra.

Another important finding that comes from analyzing of the resonance Raman profiles is that the maximum of the resonance profiles for the defective and pristine part of the nanotube does not coincide. The resonance profile of the defective part is downshifted by about 15−20 meV in photon energy with respect to the resonance maximum of the pristine part of the same tube. In addition, the resonance profile of the defective part seems to be broadened. Consequently, the Raman RBM band intensity far off resonance is quite similar for the defective and the pristine parts of the nanotube. The broadening of the resonance profile can be rationalized by the formation of a new band in the electronic density of states (midgap states) due to the defect. Additionally, defects introduce local strain, which modifies the carbon atom locations, and so forth. Consequently, a local change of the transition energy between van Hove singularities E_{ii} can be expected as the resonance profile is changed. The formation of new bands in the electronic density of states has been shown previously by STS measurements,[12] near field studies,[4] and also has been proposed by calculations.[25] These new states are presumably localized and located at the defect sites. However, the Raman spectra are collected from an area where more defects are present and therefore the resulting spectrum gives average results coming from the effects of several defect sites. These defects would lead to several new bands in the electronic structure of the nanotube and consequently they will reduce the band gap of a semiconducting tube that results in a downshift of the Raman resonance profile of the RBM on an energy scale.

A similar effect to the formation of defects (a frequency shift, broadening of the resonance Raman profiles, and a reduction in the intensity at the maximum of the resonance Raman profile) can also be a consequence of the doping of nanotubes as has been demonstrated recently by electrochemical charging of individual semiconducting/metallic nanotubes.[26] For semiconducting tubes, the effects of doping are observed at relatively large electrode potential (≥ ±0.5 V). Hence it is not likely that the effects observed here in this work are a consequence of unintentional doping.

It is interesting to explore how electrochemical charging influences the Raman features of the defective tube. This is due to a small charging that is expected to be present in the case of most samples due to the natural doping of nanotube samples from the environment, for example, by oxygen

DOI: 10.1021/nl102727f | *Nano Lett.* **2010,** *10,* 4619–4626

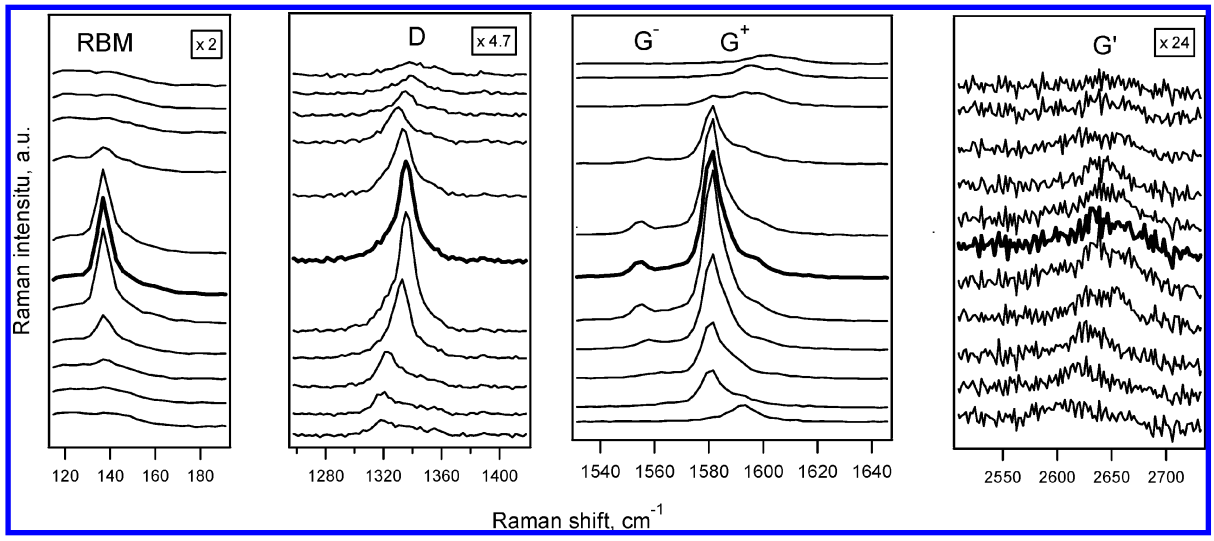

FIGURE 4. Spectroelectrochemical data on a defective part of an individual semiconducting nanotube. The potential steps are 0.3 V. The bold trace is for $V = 0$. The electrode potential is changed from 1.5 to −1.5 (top to bottom).

from the air. In the case of spectroelectrochemical measurements, doping means that a certain charge-transfer is present between a SWCNT and its environment. This charge transfer does not necessarily require the presence of covalently bonded heteroatoms in the nanotube, but can solely involve the counterions compensating the charge of the nanotube occurring in the vicinity of the SWCNT.[27] It is known that the doping of a SWCNT causes significant changes in the Raman spectra.[28] Since these changes include shifts in frequency, band shape modulations, and also attenuation/increase of various Raman bands, it is important to evaluate their complex variations with electrode potential. The role of the charging has been previously studied for nondefective samples,[26] but a detailed study of these parameters in individual defective tubes is still not available.

Figure 4 shows in situ spectroelectrochemical data obtained on a defective individual SWCNT. It is in general difficult to study the doping of defective tubes because the defects limit the conductivity and also lead to an enhanced reactivity of the nanotube. Hence only samples with a low defect density can be studied by spectroelectrochemistry.

The most significant effect of spectroelectrochemical doping is the change of the intensity of the Raman bands for each Raman feature (the RBM, the D band, the G band, and the G′ band). As shown in Figure 4, such an effect is present and it is observed for all SWCNT Raman features in individual defective SWCNTs. This behavior is similar to the case of nondefective nanotube samples.[26] The effect shown in Figure 4 is caused by the filling of the electronic states, which in turn leads to a modification of the nanotube electronic structure and results in a change (reduction in intensity) of the resonance Raman signal.

The electrode potential causing a change in the resonance Raman signal also leads to a change of the intensity of the D mode. It is often argued that the ion bombardment of SWCNTs on a substrate introduces charged impurities/local charges in the substrate, which in turn affects the SWCNT.

The reversible bleaching of the D mode in our study, however, confirms that the D band is a consequence of the defect created in the nanotube wall. Local charges in the substrate are also expected to delay the bleaching of the Raman bands. However, we do not see a significantly different behavior between the pristine and defective parts of the SWCNT. Hence, our experiments suggest that charges from the substrate do not affect our experimental results significantly. We also suggest that all charged impurities (if they are present) are removed/compensated during the electrochemical charging.

The change of the D mode intensity is also of particular importance for metrology since doping may influence the evaluation of defects in a sample. In other words, for a doped sample the intensity of the D mode is reduced compared to pristine SWCNTs and consequently the amount of defects may be underestimated if only the intensity of the D mode is considered.

For the evaluation of defects, the I_D/I_G (I denotes peak height) ratio is often used. However, this ratio is dependent on the doping level due to the change in width of the D and the G Raman bands during the doping. Therefore, A_D/A_G (A denotes the integrated area of a particular Raman mode in the Raman spectrum) is more accurate since the changes in the bandwidth do not affect this ratio. In Figure 5, we plot the A_D/A_G ratio as a function of electrode potential. It is evident that the A_D/A_G ratio increases with doping. There is only a weak variation in the range of the potential from −0.5 to about +1 V. This is consistent with previous studies showing that at least a potential equal to the first van Hove singularity must be applied to change the electronic structure of a SWCNT.[26] For potentials outside the −0.5 to +1 V region, the A_D/A_G ratio increases with increasing magnitude

DOI: 10.1021/nl102727f | Nano Lett. 2010, 10, 4619–4626

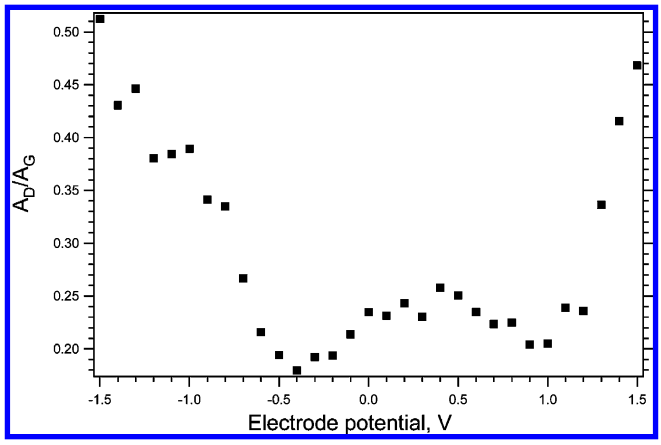

FIGURE 5. A_D/A_G ratio as a function of electrode potential for a defective part of an individual semiconducting nanotube.

of the electrode potential both for positive and negative doping. The maximum value of $A_D/A_G \approx 0.5$ was found at an electrode potential of −1.5 V. At a maximum positive potential (1.5 V) the value of A_D/A_G was slightly smaller (0.45).

For the G^+ and the D modes, we also observed a change in their peak frequencies as the electrode potential is varied (see Figure 4). The G^+ mode frequency ($\omega_G{}^+$) is upshifted with respect to its position at 0 V for both potentials larger than 0.9 V and for negative potentials lower than approximately −0.9 V. A change of $\omega_G{}^+$ was also observed for nondefective semiconducting SWCNTs as the potentials change magnitudes and signs. In the previous work[29] on five different individual nondefective semiconducting nanotubes, it was demonstrated that the sign of the frequency shift ($\delta\omega_G{}^+/\delta V_e$) is different for different tubes with regard to negative charging, but, in contrast, the sign of $\delta\omega_G{}^+/\delta V_e$ was found to be the same for positive charging.[29] It was observed that the response of the G^+ band to a potential is dependent on the SWCNT diameter: for negative charging, the large diameter tubes exhibit an upshift of the G^+ band, while the small diameter tubes exhibit a downshift of the G^+ band upon negative charging. The tube in Figure 4 has a relatively large diameter and therefore the observed upshift for both positive and negative doping is in agreement with previous results on nondefective tubes.[29]

The D mode frequency is also changed with applied electrode potential. For positive charging, we observed a decrease of ω_D and then an increase. In the case of negative doping, we observed only a decrease of ω_D. This behavior is consistent with a recent near field Raman study of phosphorus and boron-doped individual SWCNTs.[4]

In conclusion, we present a detailed study of the role of defects in the Raman spectra of individual semiconducting SWCNTs. The formation of the defect manifests itself in the appearance of the D band in the Raman spectra and by variations of other Raman features. These features exhibit a change of the energy of the resonance maximum and intensity of the resonance maximum. On the other hand, the formation of new bands or significant shifts of the RBM, the G band and the G′ band frequency were not observed.

Our results clearly show that the defective tubes contribute less to the intensity of Raman features (except the D mode, since its intensity is increasing with the amount of defects). In other words, the Raman spectra of a sample containing defective and nondefective tubes are dominated by the contribution from nondefective ones. Hence, if the defects are healed, the spectral response of the sample will change significantly, since the signal of tubes with healed defects will then contribute to the spectra more significantly to each of the RBM, the G band, and G′ band features.

Since the resonance maxima are changed by introducing defects, different tubes may contribute to the spectra at a given E_{laser} even though these tubes are not in resonance when the same (n,m) tubes are not defective.

We also show that the G′ band intensity is sensitive to the formation of the defects. For example, the G′ band decreases its intensity with the formation of defects. This effect has also important consequences for the evaluation of defects based on Raman spectroscopy. For example, the $I_D/I_{G'}$ ratio is frequently used for analysis of the amount of the defects in a given sample where the $I_{G'}$ is assumed to be a "constant" reference. However, defect formation leads to a decrease of $I_{G'}$, the $I_D/I_{G'}$ ratio will increase because of both the increase in I_D and the decrease in $I_{G'}$. Therefore the number of defects may be overestimated if the defect induced change in $I_{G'}$ is neglected.

The behavior of an individual defective nanotube has also been investigated during electrochemical charging with both positive and negative potentials. The charging leads to the reduction in the intensity of all Raman modes including the D mode, which is consistent with the results obtained previously on nondefective tubes. In particular, the reduction of the D mode intensity is important because it may lead to the underestimation of the amount of defects in doped samples if the evaluation of the number of defects is based solely on the D band intensity.

Acknowledgment. This work was supported by the Academy of Sciences of the Czech Republic (contracts Nos. 203/07/J067, IAA400400804, IAA400400911, and KAN200100801), MSMT (ME09060), M.S.D. acknowledges support from NSF/DMR-07-04197, H.F. and J.K. acknowledge the support by the Center for Excitonics, an Energy Frontier Research Center funded by the U.S. Department of Energy, Office of Science, Office of Basic Energy Sciences under Award Number DE-SC0001088. Y.P.H. acknowledges financial support from the National Science Council of the Republic of China through Project No. NSC98-2917-I-564-140. Work was carried out using the Raman facility in the MIT Spectroscopy Laboratory supported by Grants NSF-CHE 0111370 and NIH-RR02594. The authors are grateful to K. K. Berggren for helpful discussions and providing access to a UHV RF Ar plasma source.

DOI: 10.1021/nl102727f | *Nano Lett.* **2010,** *10,* 4619–4626

REFERENCES AND NOTES

(1) Khalap, V. R.; Sheps, T.; Kane, A. A.; Collins, P. G. Hydrogen Sensing and Sensitivity of Palladium-Decorated Single-Walled Carbon Nanotubes with Defects. *Nano Lett.* **2010**, *10* (3), 896–901.

(2) Dresselhaus, M. S.; Kalish, R. *Ion Implantantion in Diamond, Graphite and Related Materials*; Springer-Verlag: Berlin, 1992.

(3) Suenaga, K.; Wakabayashi, H.; Koshino, M.; Sato, Y.; Urita, K.; Iijima, S. Imaging active topological defects in carbon nanotubes. *Nat. Nanotechnol.* **2007**, *2* (6), 358–360.

(4) Maciel, I. O.; Anderson, N.; Pimenta, M. A.; Hartschuh, A.; Qian, H. H.; Terrones, M.; Terrones, H.; Campos-Delgado, J.; Rao, A. M.; Novotny, L.; Jorio, A. Electron and phonon renormalization near charged defects in carbon nanotubes. *Nat. Mater.* **2008**, *7* (11), 878–883.

(5) Skakalova, V.; Kaiser, A. B.; Dettlaff, U.; Arstila, K.; Krasheninnikov, A. V.; Keinonen, J.; Roth, S. Electrical properties of C4+ irradiated single-walled carbon nanotube paper. *Phys. Status Solidi B* **2008**, *245* (10), 2280–2283.

(6) Skakalova, V.; Maultzsch, J.; Osvath, Z.; Biro, L. P.; Roth, S. Intermediate frequency modes in Raman spectra of Ar+-irradiated single-wall carbon nanotubes. *Phys. Status Solidi RRL* **2007**, *1* (4), 138–140.

(7) Jorio, A.; Fantini, C.; Dantas, M. S. S.; Pimenta, M. A.; Souza, A. G.; Samsonidze, G. G.; Brar, V. W.; Dresselhaus, G.; Dresselhaus, M. S.; Swan, A. K.; Unlu, M. S.; Goldberg, B. B.; Saito, R. Linewidth of the Raman features of individual single-wall carbon nanotubes. *Phys. Rev. B* **2002**, *66* (11), 115411.

(8) Maultzsch, J.; Reich, S.; Schlecht, U.; Thomsen, C. High-energy phonon branches of an individual metallic carbon nanotube. *Phys. Rev. Lett.* **2003**, *91* (8), No. 087402.

(9) Souza, M.; Jorio, A.; Fantini, C.; Neves, B. R. A.; Pimenta, M. A.; Saito, R.; Ismach, A.; Joselevich, E.; Brar, V. W.; Samsonidze, G. G.; Dresselhaus, G.; Dresselhaus, M. S. Single- and double-resonance Raman G-band processes in carbon nanotubes. *Phys. Rev. B* **2004**, *69* (24), R15424.

(10) Zolyomi, V.; Kurti, J.; Gruneis, A.; Kuzmany, H. Origin of the fine structure of the Raman D band in single-wall carbon nanotubes. *Phys. Rev. Lett.* **2003**, *90* (15), 157401.

(11) Skakalova, V.; Dettlaff-Weglikowska, U.; Roth, S. Gamma-irradiated and functionalized single wall nanotubes. *Diamond Relat. Mater.* **2004**, *13* (2), 296–298.

(12) Tolvanen, A.; Buchs, G.; Ruffieux, P.; Groning, P.; Groning, O.; Krasheninnikov, A. V. Modifying the electronic structure of semiconducting single-walled carbon nanotubes by Ar+ ion irradiation. *Phys. Rev. B* **2009**, *79* (12), 125430.

(13) Tuinstra, F.; Koenig, J. L. Raman Spectrum of Graphite. *J. Chem. Phys.* **1970**, *53* (3), 1126–1130.

(14) Thomsen, C.; Reich, S. Double resonant Raman scattering in graphite. *Phys. Rev. Lett.* **2000**, *85* (24), 5214–5217.

(15) Maultzsch, J.; Reich, S.; Thomsen, C. Chirality-selective Raman scattering of the D mode in carbon nanotubes. *Phys. Rev. B* **2001**, *6412* (12), 121407 (R).

(16) Araujo, P. T.; Doorn, S. K.; Kilina, S.; Tretiak, S.; Einarsson, E.; Maruyama, S.; Chacham, H.; Pimenta, M. A.; Jorio, A. Third and fourth optical transitions in semiconducting carbon nanotubes. *Phys. Rev. Lett.* **2007**, *98* (6), No. 067401.

(17) Araujo, P. T.; Maciel, I. O.; Pesce, P. B. C.; Pimenta, M. A.; Doorn, S. K.; Qian, H.; Hartschuh, A.; Steiner, M.; Grigorian, L.; Hata, K.; Jorio, A. Nature of the constant factor in the relation between radial breathing mode frequency and tube diameter for single-wall carbon nanotubes. *Phys. Rev. B* **2008**, *77* (24), 241403.

(18) Brown, S. D. M.; Jorio, A.; Corio, P.; Dresselhaus, M. S.; Dresselhaus, G.; Saito, R.; Kneipp, K. Origin of the Breit-Wigner-Fano lineshape of the tangential G-band feature of metallic carbon nanotubes. *Phys. Rev. B* **2001**, *6315* (15), 155414.

(19) Reich, S.; Thomsen, C.; Maultzsch, J. Carbon Nanotubes: Basic Concepts and Physical Properties. In *Carbon Nanotubes: Basic Concepts and Physical Properties*; Wiley-VCH: Berlin, 2004; p 153.

(20) Kalbac, M.; Kavan, L.; Dunsch, L. Selective Etching of Thin Single Wall Carbon Nanotubes. *J. Am. Chem. Soc.* **2009**, *131* (12), 4529–4534.

(21) Hofmann, M.; Nezich, D.; Reina, A.; Kong, J. In-Situ Sample Rotation as a Tool to Understand Chemical Vapor Deposition Growth of Long Aligned Carbon Nanotubes. *Nano Lett.* **2008**, *8* (12), 4122–4127.

(22) Lucchese, M. M.; Stavale, F.; Ferreira, E. H. M.; Vilani, C.; Moutinho, M. V. O.; Capaz, R. B.; Achete, C. A.; Jorio, A. Quantifying ion-induced defects and Raman relaxation length in graphene. *Carbon* **2010**, *48* (5), 1592–1597.

(23) Popov, V. N.; Lambin, P. Theoretical resonant Raman spectra of nanotube (7,0) with point defects. *Phys. Status Solidi B* **2009**, *246* (11−12), 2602–2605.

(24) Popov, V. N.; Lambin, P. Resonant Raman intensity of the totally symmetric phonons of single-walled carbon nanotubes. *Phys. Rev. B* **2006**, *73* (16), 165425.

(25) Okada, S. Energetics and electronic structures of carbon nanotubes with adatom-vacancy defects. *Chem. Phys. Lett.* **2007**, *447* (4−6), 263–267.

(26) Kalbac, M.; Farhat, H.; Kavan, L.; Kong, J.; Sasaki, K.; Saito, R.; Dresselhaus, M. S. Electrochemical charging of individual single-walled carbon nanotubes. *Acs Nano* **2009**, *3* (8), 2320–2328.

(27) Kavan, L.; Dunsch, L. Spectroelectrochemistry of carbon nanostructures. *ChemPhysChem* **2007**, *8* (7), 975–998.

(28) Freitag, M.; Tsang, J.; Avouris, P. Local measurement of charge density in carbon nanotubes by Raman spectroscopy. *Phys. Status Solidi B* **2008**, *245* (10), 2216–2220.

(29) Kalbac, M.; Farhat, H.; Kavan, L.; Kong, J.; Dresselhaus, M. S. Competition between the Spring Force Constant and the Phonon Energy Renormalization in Electrochemically Doped Semiconducting Single Walled Carbon Nanotubes. *Nano Lett.* **2008**, *8* (10), 3532–3537.

DOI: 10.1021/nl102727f | *Nano Lett.* **2010,** *10,* 4619–4626